doi:10.14311/ppt.2023.1.15
Plasma Physics and Technology **10**(1):15–19, 2023

RADIATIVE HEAT TRANSFER IN MODELS OF DC ARC PLASMA

M. Baeva[a,*], P. Kloc[b], Y. Cressault[c]

[a] *Leibniz Institute for Plasma Science and Technology, 17489, Greifswald, Germany*
[b] *Brno University of Technology, Brno, 61600, Czech Republic*
[c] *LAPLACE, Université de Toulouse, CNRS, UPS, INPT, 31062, France*
[*] baeva@inp-greifswald.de

Abstract. The radiative heat transfer in arc plasma models of a free-burning arc and a plasma torch in atmospheric pressure argon is taken into account in a self-consistent way. This is realized by the P_1 method for solving the equation of radiative transfer and the multi-band approximation that considers the division of the emitted spectrum into a number of spectral bands. Net emission coefficients are evaluated by solving the equation of radiative transfer in three dimensions in an isothermal cylindrical plasma. The arc plasma parameters of the free-burning arc and the plasma torch obtained accounting for radiative transport have been compared with those from the temperature-dependent net emission coefficient for a radius of 1 mm. The results show that in general, the models applying the net emission coefficient provide results in the arc core close to that using the P_1 method. The discrepancy is stronger in the arc periphery and near walls, where the P_1 method predicts absorption of radiation.

Keywords: radiative heat transfer, arc plasma, equilibrium, multi-band approximation, P_1 method, net emission coefficient.

1. Introduction

The radiative heat transfer represents the interaction between the radiation and the plasma matter and is an important cooling mechanism of electric arcs. Arc plasmas are heated up to temperatures of tens of thousands of kelvin that implies irradiation by neutral and charged particles covering the frequency region $\nu \sim (10^{12} - 10^{16})$ Hz, where thousands of spectral lines exist. The change of the spectral radiative intensity along a line of sight due to emission and absorption is governed by the equation of radiative transfer (ERT) with account for the spatial distributions of temperature, pressure, and the plasma composition. The computation of the radiative heat flux for every frequency and direction in space within the arc model is hardly affordable and simplifications are usually introduced. A common approach used in many arc models makes use of a net emission coefficient (NEC) [1] obtained for an isothermal cylinder of a given radius. This approach is often reduced to the computation of the radiative heat losses in the arc as a function of the local values of temperature and pressure although NEC is strongly speaking determined by the entire temperature profile in the arc [1].

A simplification that ensures a self-consistent access to the radiative heat transfer in arc plasma models implies a division of the spectrum into a number of bands [2]. In each band, an average absorption coefficient is defined, e.g. as Planck or Rosseland means or a hybrid of both [3]. Then, a P_1-approximation of the method of spherical harmonics or the discrete ordinate method (DOM) [2] is implemented into the arc model. This approach is followed in this study, which is concerned with the influence of the description of the radiative heat transfer in models of arc plasma in the state of local thermodynamic equilibrium (LTE).

2. Physical background

The basic model that couples an arc plasma in LTE, the thermionic cathode and its non-equilibrium boundary layer has been reported elsewhere [4]. It solves the Navier-Stokes equations for conservation of mass, momentum, and energy for a compressible fluid, current continuity and Maxwell equations, Ohm's law, and equation of state. In this work, we focus on the description of the radiative heat transfer as a part of the energy balance of the arc plasma. The equation of energy conservation of the LTE plasma reads

$$\rho C_p \mathbf{u}\cdot\nabla T + \nabla\cdot(\mathbf{q}+\mathbf{q}_\mathrm{r}) = \alpha_p T \mathbf{u}\cdot\nabla + \hat{\tau} : \nabla\mathbf{u} + Q. \quad (1)$$

In Eq. (1), ρ is the mass density, C_p is the specific heat capacity at constant pressure, T is the plasma temperature, $\mathbf{u}$ is the velocity vector, $\mathbf{q}$ is the conductive heat flux, $\mathbf{q}_\mathrm{r}$ is the radiative heat flux, $\alpha_p = -\frac{1}{\rho}\frac{\partial\rho}{\partial T}$ is the coefficient of thermal expansion, p is the pressure, $\hat{\tau}$ is the viscous stress tensor for a Newtonian fluid, and Q contains heat sources others then pressure work and viscous dissipation. These sources are the Joule heating $\mathbf{j}\cdot\mathbf{E}$ and the electron enthalpy $\frac{5k_B}{2e}\mathbf{j}\cdot\nabla T$ with $\mathbf{j}$ and $\mathbf{E}$ being the electric current density and the electric field strength, respectively. Eq. (1) can be rewritten with the radiative heat flux representing the radiative losses $-Q_\mathrm{r} = -\nabla\cdot q_\mathrm{r}$ on the right-hand-side (r.h.s). Further, $\mathbf{q}_\mathrm{r}$ couples Eq. (1) with the ERT. In

the case scattering is neglected, the ERT reads [2]

$$\frac{\mathrm{d}I_s}{\mathrm{d}s} = \kappa_\nu B_\nu - \kappa_\nu I_\nu. \tag{2}$$

In Eq. (2), I_ν is the spectral radiative intensity along a line of sight in direction $\mathbf{s}$, κ_ν is the spectral absorption coefficient, $B_\nu = \frac{2h}{c^2}\frac{\nu^3}{\exp(h\nu/k_BT)-1}$ is the Planck function, and h and k_B are respectively the Planck and Boltzmann constants. The integration of the ERT over all directions yields

$$\nabla\cdot\mathbf{q}_{r\nu} = 4\pi\kappa_\nu B_\nu - \int_{\Omega=0}^{4\pi}\kappa_\nu I_\nu \mathrm{d}\Omega. \tag{3}$$

Integration over the spectrum provides the term $\nabla\cdot\mathbf{q}_\mathrm{r}$ that is included in Eq. (1) of the arc model.

Many models of LTE arc plasma employ the NEC [1] and express the divergence of radiative flux as $\nabla\cdot\mathbf{q}_\mathrm{r} = 4\pi\varepsilon_N$. In this work, the ERT (2) is solved along with the equations of the arc model. The solution of Eq. (2) is based on the method of spherical harmonics in its lowest approximation P_1. In this approximation, the governing equations become [2]

$$\nabla\cdot\mathbf{q}_\mathrm{r} = \kappa\big[4\pi B - G(\mathbf{r})\big], \tag{4}$$

$$\mathbf{q}_\mathrm{r} = -\frac{1}{3\kappa}\nabla G(\mathbf{r}), \tag{5}$$

where $G(\mathbf{r}) = \int_{\Omega=0}^{4\pi}\kappa_\nu I_\nu \mathrm{d}\Omega$ is the incident radiation. The boundary condition at opaque walls reads

$$\mathbf{n}\cdot\left(-\frac{1}{3\kappa}\nabla G(\mathbf{r})\right) = q_\mathrm{r,net}, \tag{6}$$

with $q_{r,net}$ being the net radiative flux absorbed by the boundary and $\mathbf{n}$ is the surface normal. Depending on the surface emissivity ϵ in the range (0,1), the boundary is treated as gray and $q_\mathrm{r,net} = \frac{\epsilon}{2(2-\epsilon)}[4\pi B\eta - G]$ or black ($\epsilon = 1$). η accounts for the fractional emissive power in a given spectral interval. The net radiative flux at flow inlets and outlets is computed in the same manner as at walls assuming emissivity of one.

The absorption coefficient κ in Eq. (4) is introduced as spectral absorption coefficient applying the multi-band approximation. It implies a set of frequency intervals with a uniform value of the absorption coefficient κ_ν in each interval [2]. The number of frequency intervals and their boundaries are chosen with respect to the behaviour of the absorption coefficient. Five intervals with boundaries 0.003, 1.0, 2.8, 3.8, 6.67, and 10.0 in units of 10^{15} Hz as reported in [5] are used in the present work. The evaluation of the spectral absorption coefficient κ_ν in each interval of frequencies $[\nu_i, \nu_{i+1}]$ can be performed applying Plank (κ_P) or Rosseland (κ_R) averaging [2] or a combination of both (κ_h) that leads to a hybrid mean value [3]. The idea behind the hybrid mean absorption coefficient is to weight the overestimate and the underestimate

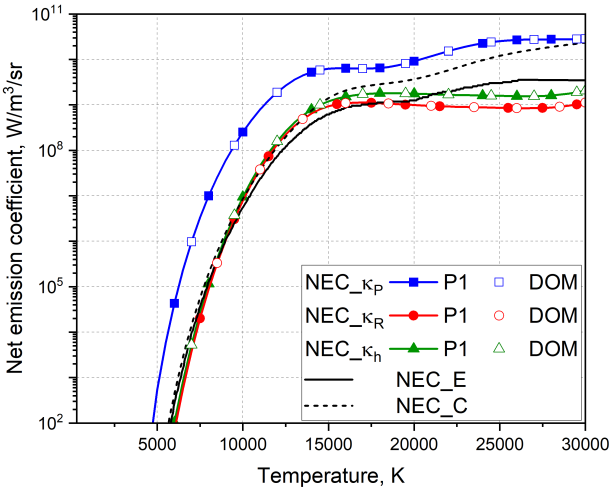

Figure 1. Net emission coefficients ε_N from the P_1, DOM-methods and a 5-band approximation applying Planck (NEC_κ_P), Rosseland (NEC_κ_R), and hybrid (NEC_κ_h) mean spectral absorption coefficients. NEC_E [10] and NEC_C [11] are published data.

expected by respectively the Plank and Rosseland mean absorption coefficients. The equations read

$$\kappa_\mathrm{P} = \int_{\nu_i}^{\nu_{i+1}}\kappa_\nu B_\nu \mathrm{d}\nu \Big/ \left[\int_{\nu_i}^{\nu_{i+1}} B_\nu \mathrm{d}\nu\right] \tag{7}$$

$$\kappa_\mathrm{R}^{-1} = \int_{\nu_i}^{\nu_{i+1}}\kappa_\nu^{-1}\frac{\mathrm{d}B_\nu}{\mathrm{d}T}\mathrm{d}\nu \Big/ \left[\int_{\nu_i}^{\nu_{i+1}}\frac{\mathrm{d}B_\nu}{\mathrm{d}T}\mathrm{d}\nu\right] \tag{8}$$

$$\kappa_\mathrm{h} = \gamma\kappa_\mathrm{R} + (1-\gamma)\kappa_\mathrm{P}, \tag{9}$$

with $\gamma = (\kappa_\mathrm{P} - \kappa_\mathrm{R})/\kappa_\mathrm{P}$. κ_h could become negative if $\kappa_\mathrm{R}/\kappa_\mathrm{P} > 2$. In case of argon this is not the case.

The spectral absorption coefficient κ_ν is obtained taking into account bound-bound (atomic and ionic lines), bound-free (photoionization continuum), and free-free (bremsstrahlung) processes. In total, 804 atomic and ionic lines (412 for ArI, 300 for ArII, 68 for ArIII and 24 for ArIV) from the NIST database are included [6]. Doppler, Stark, Van der Waals, and resonance broadening are considered for the spectral lines. The final line profile is obtained employing an approximation to the Voigt line profile [7]. The evaluation of the photoionization is based on cross section data from the Opacity Project and the hydrogenic approximation [8] in the case of missing data. The bremstrahlung contribution is calculated for neutral atoms and ions of argon. The frequency range $(1\cdot10^{11} - 1.2\cdot10^{16})$ Hz is divided by 1199991 frequency-grid points to ensure a step of 10^{10} Hz. Notice that the data used in this work differs from that in [9]. An analysis of the influence of the database on the model's predictions will be considered in a forthcoming work.

NECs are evaluated by solving the ERT (2) for an isothermal cylinder of radius $R = 1$ mm by means of the P_1-method and DOM, and the 5-band approximation for plasma temperatures of up to 30000 K. The predictions of the arc plasma model with implementation of the ERT can be then compared with those of

the model employing NEC. Fig. 1 shows the results for the NECs obtained with Planck (NEC_κ_P), Rosseland (NEC_κ_R), and hybrid means (NEC_κ_h) of the spectral absorption coefficient according to Eqs. (7) along with published data NEC_E [10] and NEC_C [11]. The NECs implying the mean κ_P-values and the κ_R-values are respectively the largest and the lowest. The result NEC_κ_R agrees well with NEC_E and NEC_C for temperatures up to 17000 K. For higher temperatures, the deviation from NEC_C becomes stronger. The introduction of the hybrid mean absorption coefficient κ_h reduces the deviation between NEC_κ_R and NEC_E in particular for temperatures above 20000 K. Notice that the NECs obtained by the P_1-method and DOM practically do not differ.

3. Results

This work sets the focus on models of a free-burning arc and a plasma spray torch operated in argon at atmospheric pressure. The P_1-method (Eqs. (4)) with the 5-band approximation of the hybrid mean absorption coefficient are implemented to solve the ERT (2) along with the equations of the arc plasma model [4]. In addition, the radiative loss term in Eq. (1) has been expressed in terms of NEC and simulations are performed for the sake of comparison. The NEC for argon at atmospheric pressure is based on the 5-band approximation and the hybrid mean value κ_h, and the solution of the ERT (2) for an isothermal cylinder with a radius of 1 mm. The NEC is computed prior to the simulation (see Fig. 1). Both arc models are realized as two-dimensional and axisymmetric. Forthcoming works will consider three-dimensional geometries and the implementation of the DOM.

The model of the free-burning arc employs a tungsten-inert gas arrangement with a La-W cathode (20 mm length, 1.6 mm radius, truncated 60° conical tip with a radius of 0.3 mm). The anode is a water-cooled cooper plate with a radius of 25 mm and a thickness of 8 mm. The distance between the cathode tip and the anode is 3 mm. Direct current (DC) of 100 A and a flow rate of 12.6 NLPM are applied.

The model of the plasma spray torch is based on the DC plasma torch F4MB-XL by Oerlikon-Metco in a steady operating mode. The cathode is made of La-W (radius of the cylindrical part 4.9 mm, a rounded tip with a radius of 1.9 mm). The nozzle (anode) has a conical part through which the gas is fed and a cylindrical part with a radius of 3 mm and a length of 20 mm. The torch is operated with a flow rate of 40 NLPM and a DC current of 600 A.

Figures 2 and 3 present the distribution of the arc plasma temperature T and the radiative loss term Q_r for the free-burning arc and for the plasma torch, respectively. Each graph contains the results obtained by both the NEC and the P_1 approaches. The NEC results are presented by uniform coloured lines taken at the corresponding contour values, while the P_1

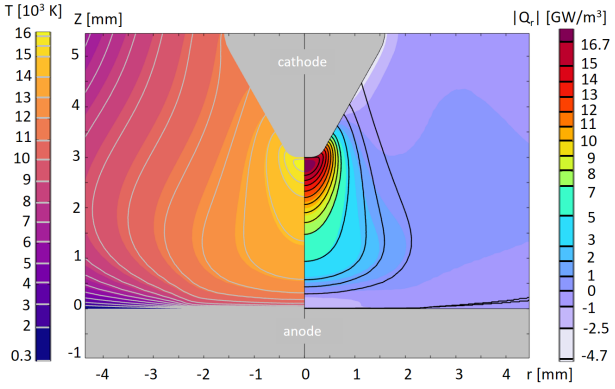

Figure 2. Contours of equal T (l.h.s) and Q_r (r.h.s.) from the free-burning arc models with NEC (contour lines) and P_1 (filled contours).

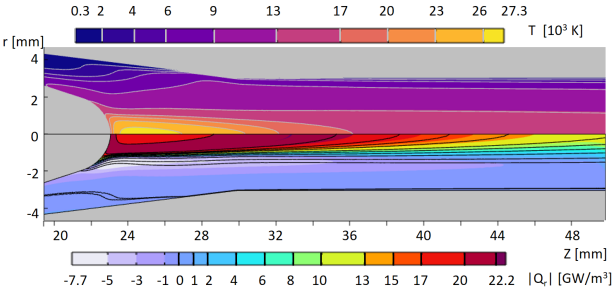

Figure 3. Contours of equal T (top) and Q_r (bottom) from DC torch arc models with NEC (contour lines) and P_1 (filled contours)

results are presented as filled contours in a colour map. Different colour maps are chosen for T and Q_r for the sake of a better data reading. The contour lines overlap with the edge between two filled contours in the case of coinciding data. The operating conditions are chosen in a way that cases of different maximum plasma temperatures are covered – about 16200 K in the free-burning arc and about 27200 K in the DC torch. The behaviour of the T, Q_r, and the axial flow velocity w along the axis of symmetry is shown in Figures 4 and 5 for respectively the free-burning arc and the DC torch.

In the free-burning arc, close to the cathode tip, i.e. in the region of maximum plasma temperature, the NEC and the P_1 approaches deliver almost the same results for T. The solutions separate from each other in the arc fringes. The values of Q_r from the model with P_1 are slightly higher in the hot arc core. Q_r becomes negative in the region surrounding the upper part of the cathode and close to the anode (Figs. 2 and 4). The values of Q_r from the model with NEC are slightly higher than those from P_1. The discrepancy in the axial flow velocity is very small.

In the DC torch, the NEC ($R = 1$ mm) and the P_1 approaches predict almost the same Q_r values in the hottest plasma region but downstream those in the NEC ($R = 1$ mm) approach become lower. This difference hardly influences the plasma temperature so that T from both models is almost the same (see

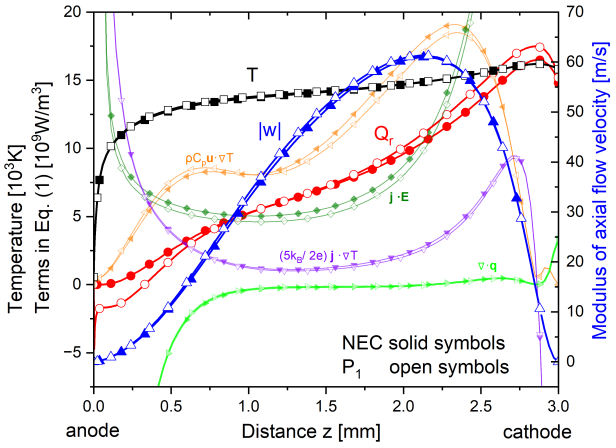

Figure 4. Axial distributions of the plasma temperature T, the modulus of axial velocity $|w|$, and terms in Eq. (1) in the free-burning arc.

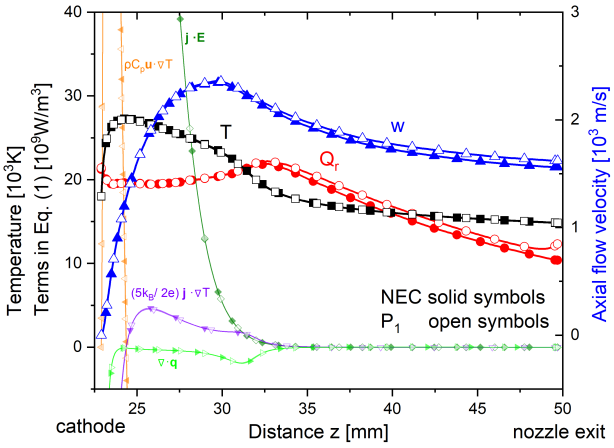

Figure 5. Axial distributions of the plasma temperature T, the axial velocity w, and terms in Eq. (1) in the DC torch.

Figs. 3 and 5). The discrepancy in the flow velocity is less than 3% due to the high flow velocity in the DC torch. The model with P_1 indicates negative Q_r values along the nozzle wall (the anode). The absorption of radiation is strongest for radial position of about 2 mm and axial positions 23–33 mm.

In general, the results show that NEC ($R = 1$ mm) is a good choice for the models of the free-burning arc and the DC torch. Since the data set for the spectral absorption coefficient employed in this work differs from that in [9], in particular in the number of spectral lines, the present results also differ in some extend. As a matter of fact, the Q_r values in the hottest region of the DC torch are by a factor of two lower in the present work than in [9] although maximum plasma temperature of about 27200 K is obtained in both works. The reason is probably related to the strong convective effects in the DC torch.

The small differences in the Q_r values from the arc models with NEC and P_1-methods are not necessarily resulting from small Q_r values. Additional terms from Eq. (1) are shown in Figures 4 and 5. It can be seen that the Joule heating ($\mathbf{j}\cdot\mathbf{E}$) is the dominant term close to the cathode but it is less than Q_r in the most of the arc column. The convective term $\rho C_p \mathbf{u}\cdot\nabla T$ exceeds Q_r but is comparable with Q_r in the free burning arc. In the DC torch, $\rho C_p \mathbf{u}\cdot\nabla T$ reaches a maximum in the vicinity of the cathode. The transport of electron enthalpy ($\frac{5k_B}{2e}\mathbf{j}\cdot\nabla T$) and the conductive heat term $\nabla\cdot q$ is less than Q_r in both arc plasmas. The terms corresponding to viscous dissipation and pressure work are of minor importance and are not shown.

4. Conclusions

A self-consistent access to the radiative heat transfer in arc plasma models of a free-burning arc and a DC plasma torch has been realized. The deviations between the NEC and P_1-based models are stronger pronounced in the arc periphery and near electrodes/walls, where radiation is absorbed but not taken into account in the NEC-based models. Nevertheless, the NEC method ($R = 1$ mm) provides results for the arc core that are in a good agreement with those from models with the P_1 method for both the free-burning arc and the DC torch.

Acknowledgements

This work was funded in part by the European Union and the Federal State of Germany Mecklenburg-Western Pomerania (Project number TBI-V-1-321-VBW-112).

References

[1] J. J. Lowke. Predictions of arc temperature profiles using approximate emission coefficients for radiation losses. *JQSRT*, 14:111–122, 1974. doi:10.1016/0022-4073(74)90004-1.

[2] M. F. Modest. *Radiative heat transfer*. Elsevier Inc., Amsterdam, 2013. ISBN 978-0-12-386990-6.

[3] S. Kozu, T. Fijino, T. Yoshino, and T. Mori. Radiative transfer calculation of co2 thermal plasma using a hybrid plack-rosseland mean absorption coefficient. Proc. 22nd Int. Conf. Gas Discharges and Their Applications, Novi Sad, Serbia, 2018.

[4] M. Baeva, T. Zhu, T. Kewitz, et al. Self-consistent cathode-plasma coupling and role of the fluid flow approach in torch modelling. *J Therm Spray Technol*, 30:1737–1750, 2021. doi:10.1007/s11666-021-01261-4.

[5] M. Bartlova, N. Bogatyreva, and V. Aubrecht. Radiation heat transfer in thermal argon plasma with iron vapours. *Plasma Phys Technol*, 1:8–10, 2014.

[6] P. Kloc. Recent update with NIST spectral data.

[7] E. E. Whiting. An empirical approximation to the Voigt profile. *JQSRT*, 8:1379–1384, 1968. doi:10.1016/0022-4073(68)90081-2.

[8] R. W. Liebermann and J. J. Lowke. Radiation emission coefficients for sulfur hexafluoride arc plasmas. *JQSRT*, 16:253–264, 1976. doi:10.1016/0022-4073(76)90067-4.

[9] M. Baeva, Y. Cressault, and P. Kloc. Self-consistent access to radiative heat transfer in arc plasma models. Proc. 23nd Int. Conf. Gas Discharges and Their Applications, Greifswald, Germany, 2023.

[10] A. Essoltani, P. Proulx, M. Boulos, and A. Gleizes. Volumetric emission of argon plasmas in the presence of vapors of Fe, Si, and Al. *Plasma Chem Plasma Process*, 14:437–450, 1994. doi:10.1007/BF01570206.

[11] Y. Cressault and A. Gleizes. Thermal plasma properties for Ar–Al, Ar–Fe and Ar–Cu mixtures used in welding plasmas processes: I. Net emission coefficients at atmospheric pressure. *J Phys D: Appl Phys*, 46:415206, 2013. doi:10.1088/0022-3727/46/41/415206.